

PROCEEDINGS OF SPIE

SPIDigitalLibrary.org/conference-proceedings-of-spie

Protecting a fragile giant: seismic design, analysis, results and requirements for the GMT

Schwartz, Dave, Ranka, Trupti, Ashby, Dave

Dave Schwartz, Trupti Ranka, Dave Ashby, "Protecting a fragile giant: seismic design, analysis, results and requirements for the GMT," Proc. SPIE 11450, Modeling, Systems Engineering, and Project Management for Astronomy IX, 114500S (13 December 2020); doi: 10.1117/12.2560576

SPIE.

Event: SPIE Astronomical Telescopes + Instrumentation, 2020, Online Only

Protecting A Fragile Giant: Seismic Design, Analysis, Results and Requirements for the GMT

Dave Schwartz^a, Trupti Ranka^a, and Dave Ashby^a

^aGiant Magellan Telescope Observatory, Pasadena, CA, USA 91107

ABSTRACT

The primary mirror of the Giant Magellan Telescope (GMT) consists of seven 8.4-meter diameter borosilicate segments. While this design has optical advantages, the unmitigated seismic risk is significant. Recently added design features meet this challenge. A 2D seismic isolation system decouples the telescope from horizontal ground motion and dampers at the interface with the primary mirror segments attenuate their motion. A detailed analysis framework has been developed to justify and refine the design. Discrete analyses, in which the models are exercised at discrete seismic intensity levels, are used to generate requirements throughout the telescope via a seismic response spectrum approach. Risk-based analyses utilize a broad characterization of uncertainty to assess probability of survival of the most critical components. These tools support a general design strategy that effectively trades the cost of designing and constructing the telescope against the seismic risk.

Keywords: probability analysis, single friction pendulum, seismic analysis, isolation, glass stress, glass failure, Weibull, uncertainty quantification

1. INTRODUCTION

Large optical observatories are built in locations that offer the best atmospheric conditions for science. These locations, such as Hawaii and Chile, are exposed to large earthquakes. Consequently, the risk of damage from one of these events is one of the driving design considerations for any large telescope.¹ The size of the new generation of Extremely Large Telescopes increases the risk relative to smaller legacy telescopes, requiring creative design solutions.²⁻⁴ In the case of the Giant Magellan Telescope (GMT), the risk is mitigated by seismic isolation at the telescopes base and the addition of dampers to the primary mirror support system. Other telescope designs have been assessed using a maximum considered earthquake at a discrete intensity level. While this is an efficient method to validate a design, the nature of earthquakes is inherently uncertain. No matter how intense the selected motion considered is, it is always possible that a more vigorous earthquake may be experienced. The GMT Organization (GMTO) has instead chosen to perform a probabilistic risk analysis for its most critical components. This analysis attempts to account for all sources of uncertainty to determine failure in probabilistic terms. This allows the project to trade cost against risk as part of the design strategy. This paper describes the many aspects of that design strategy, including the requirements, design, analysis, and recent key results.

System level seismic requirements define the necessary performance of the observatory and are covered in Section 2. The design of the telescope, in response to these requirements, is covered in Section 3. Single friction pendulum bearings decouple the horizontal ground motion at the ground level from the motion of the telescope, and the support system for the primary mirrors is engineered to distribute and dampen the load experienced by the segments. Detailed modeling and analysis is performed to calculate the seismic risk and flow down requirements to subsystems as covered in Sections 4 and 5. A direct calculation of the probability of failure of the primary mirror glass shows that the design is sufficient even though the results at the discrete maximum level were uncertain. A similar calculation for the seismic isolators also suggests the design is sufficient, and additional features can be added to the design if the risk needs to be reduced further. The design process is ongoing, and what is presented in this paper is a snapshot in an evolving design. Going forward, GMT has the tools it needs to build a cost-effective but low risk design.

Further author information:

Dave Schwartz: E-mail: dschwartz@gmto.com

Modeling, Systems Engineering, and Project Management for Astronomy IX, edited by George Z. Angeli,
Philippe Dierickx, Proc. of SPIE Vol. 11450, 114500S · © 2020 SPIE
CCC code: 0277-786X/20/\$21 · doi: 10.1117/12.2560576

Proc. of SPIE Vol. 11450 114500S-1

2. KEY SYSTEM LEVEL SEISMIC REQUIREMENTS

In most cases, GMTO has defined a required level of performance in response to discrete earthquake levels: rigidity-level earthquake (RLE), operational-level earthquake (OLE) and survival-level earthquake (SLE), which correspond to average return periods of 2, 100 and 2475 years, respectively. The RLE defines the level of ground motion below which the observatory is insensitive, and may return immediately to science operations following the event. The performance of an element in response to an OLE or SLE event depends on its criticality. Those elements that are considered onerous to replace (too expensive or otherwise impractical to replace) are expected to be undamaged by an OLE and recoverable following a SLE. Less critical elements may not be recoverable following an SLE event, but they must not pose a hazard to personnel or other elements. This approach is best applied to elements that can be built with generous design margins to ensure the specified level of performance.

In some cases, GMTO has elected to specify the probability of failure over the observatory's 50-year operation service life. This second methodology lends itself to statistical failure modes, such as crack propagation in brittle materials like glass, and displacement exceedance in nonlinear systems, such as the seismic isolation system or primary mirror supports. The principal advantage of this approach is that the hazard exposure is quantified, and thus may be monetized and weighed against the cost of additional mitigation. GMTO may then forego further mitigation should the mitigation cost exceed the monetized hazard exposure. GMTO has defined the tolerable probability of failure in the primary mirror to be 1.0%, which is roughly equivalent to the risk exposure implied by glass stress limits used for legacy telescopes built with similar optics. The tolerable probability of failure of the GMT seismic isolation system (principally displacement exceedance), is 0.5%. It is possible that these key failure tolerances will be adjusted to maintain the balance between the monetized hazard exposure and the seismic mitigation costs.

While the GMT system-level seismic requirements lead to mitigations aimed at controlling the hazard exposure, such mitigations cannot be allowed to significantly degrade telescope performance in terms of pointing, tracking or active optics.

3. DESIGN

The GMT design is divided into subsystems as illustrated in Figure 1. The telescope pier (labelled "Isolated Telescope Pier") is a reinforced concrete structure that supports the 2,300 metric ton telescope. The telescope, consists of the mount along with a set of payloads that include the principal optics and scientific instruments. The mount is a steel structure with numerous mechanisms, including three principal axes: azimuth, elevation and field rotation.

The bulk of the mount is a lightly damped steel structure with dominant modal frequencies between 3Hz and 12Hz. Additionally, when inactive, the primary mirror segments rest on a system of elastic static supports that yield a rigid-body modal frequency of approximately 10Hz. Given that the SLE spectral acceleration peaks at about 6Hz (See Figure 8), the mount structure and primary mirror static supports are expected to greatly amplify the already vigorous seismic ground motion. Additionally, the azimuth and elevation axes utilize hydrostatic bearings, which are susceptible to uplift, further aggravating the telescope's sensitivity to seismic ground motion.

To help combat these challenges, GMTO has introduced a seismic isolation system (SIS) at the base of the telescope pier to decouple horizontal seismic ground motion (see Section 3.3), and aggressive dampers at the primary mirror supports to dissipate energy (see Section 3.2). While the remaining mount payloads also require seismic considerations, they are beyond the scope of this paper.

3.1 Primary Mirror (M1)

Before discussing the mitigation features in the design, it is helpful to discuss the most critical hardware the design is protecting: the primary mirror. The GMT primary mirror is a system of seven segments, one center segment and six identical off-axis segments. The segments, each 8.4-meters in diameter, combine to form the equivalent of a 25-meter diameter monolithic primary mirror. The segments, which are made of Ohara E6 low expansion borosilicate glass, benefit from a legacy of successful mirrors produced by University Of Arizona's Richard F. Caris Mirror Lab. The 17 metric ton off-axis segments, shown in profile in Figure 2, are 80% lighter than an equivalent solid mirror due their honeycomb structure. Though the mirror segments are very stiff, the

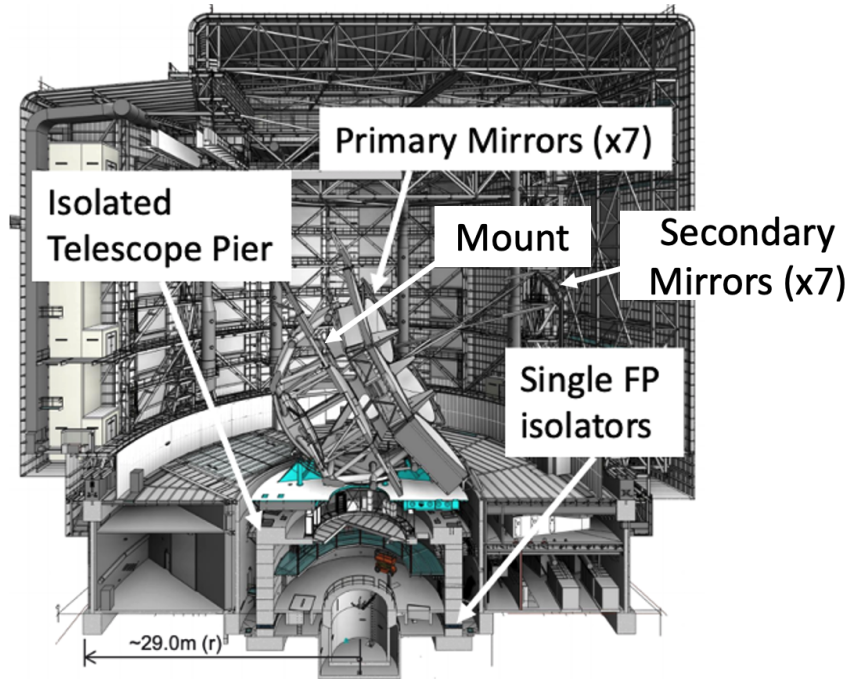


Figure 1. The Giant Magellan Telescope inside its enclosure.

25 mm thick face sheet and back plate along with the 12 mm honeycomb walls make them relatively fragile when compared to solid meniscus mirrors, particularly with regard to point loading. Most exposed surfaces are polished, which greatly increases resilience against cracks, but interior surfaces remain rough. Any significant defects are acid etched and/or ground and polished to ensure sufficient stress tolerance. A more detailed discussion of the stress and failure statistics in the glass can be found in Section 4.4.

The back of an off-axis segment is illustrated in Figure 3. Each hexagonal core features a hole to facilitate the force-air convective ventilation of the core interior, which results in uniform cooling of the segment. Several hundred pucks are adhesively attached to the back of each segment. These pucks serve to couple support loads into mirror, either individually, or in groups using 2, 3 or 4-puck loadspreaders. Because the pucks are susceptible to failure under moment loads, static supports are only coupled through 3-puck and 4-puck loadspreaders, while active support loads are coupled through both loadspreaders and individual pucks. Stiff position references are provided by the 6 hardpoint wedges, which are also adhesively attached at the back of each segment.

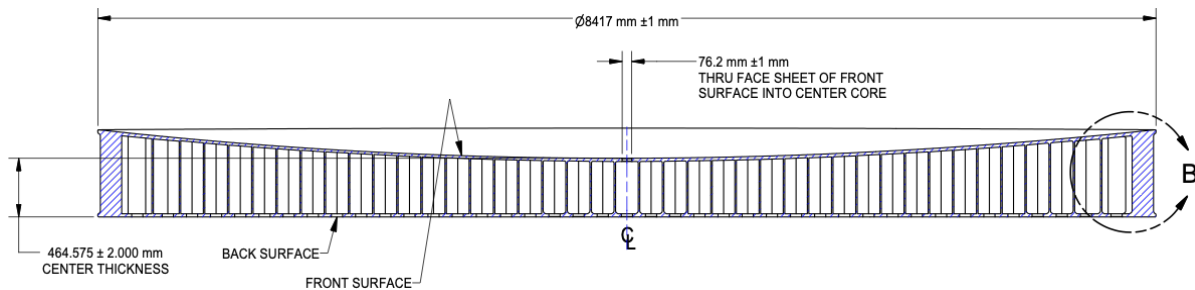


Figure 2. Profile of an off axis primary mirror segment.

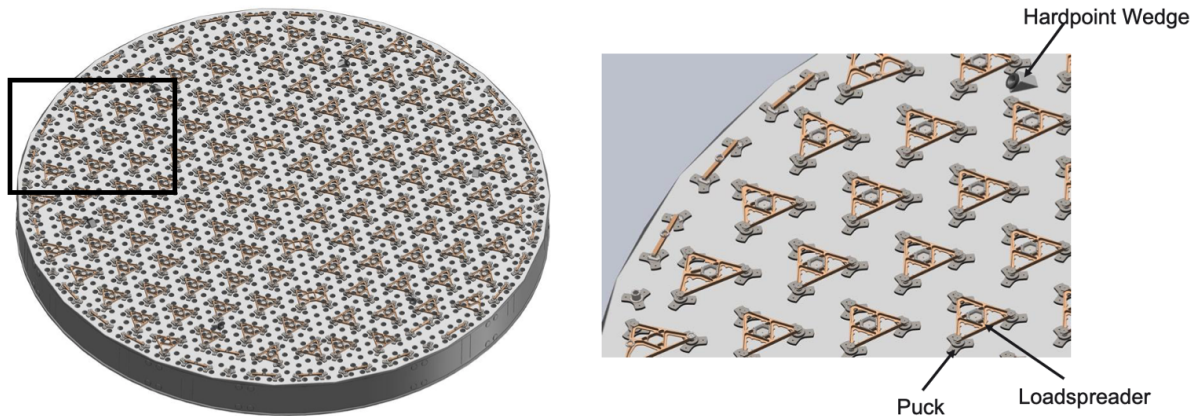


Figure 3. Back surface of an off axis primary mirror segment with interfaces to the M1 support system.

3.2 M1 Support System

When in active operation, a set of precision pneumatic support actuators (see Figure 4) uniformly carry the weight of the primary mirror segments. The support actuators also apply forces to correct shape errors on the face sheet. To facilitate variable mirror orientations, many of the support actuators are triple-axis, allowing them to apply a support force in any arbitrary direction. The support actuators apply forces, and they lack inherent stiffness, so each segment position is controlled by a stiff set of 6 hardpoints, each of which controls one positional degree of freedom. The axial force applied by the hardpoints to the mirror is limited by a pneumatic breakaway mechanism that reduces the hardpoint stiffness to zero when the axial force is larger than modestly determined threshold. Collectively, this system of support actuators and hardpoints is referred to as the active supports.

When the active supports are disabled (such as during a seismic event), the support actuators and hardpoints are depressurized so that the mirror segment comes to rest on a set of wire rope spring isolators (see Figure 5), that are collectively referred to as the static supports. When the active supports are operational, there is no contact with the static supports. This is accomplished by maintaining an air gap between the load spreader and the static supports.

The static supports must be sufficiently compliant to accommodate assembly tolerances along with gravity and thermal deformations of the mirror cell without exceeding the continuous stress tolerances of the mirror segment. They must also be stiff enough to limit the mirror segment displacement with respect the mirror cell during a seismic event so that the support actuators, hardpoints, and static supports themselves can accommodate the mirror motion without exceeding their motion capacity. Consequently, the mirror segment resting on the static supports has a lowest modal frequency of approximately 10Hz. Unfortunately, there is significant coupling between the mirror modes and the telescope mount modes, which results in a great deal of ground motion amplification. GMTO has elected to add dampers to the primary mirror support actuators to limit this amplification. The M1 Damper is located inside of the air cylinder of the support actuator. A proposed design is shown on the right hand side of Figure 4. It is specified to apply a force in the axial direction proportional to the velocity, and are active even when the support actuators are depressurized.

An individual static support isolator is shown in Figure 5. The blue arrows indicate the air gap that allows the mirror to move freely when supported in the active mode. The red arrows indicate the axial and lateral motion limits. If these limits are exceeded the risk of damage to the primary mirror increases significantly. Displacement exceedance is among the most significant concerns with regard to the primary mirror segment seismic response. Thus, displacement is a key output of the seismic models. The key seismic design challenge for the primary mirror support system is to choose parameters that balance the risk of exceeding the stroke of the system and the risk of damaging the mirror through excessive force within the stroke limits.

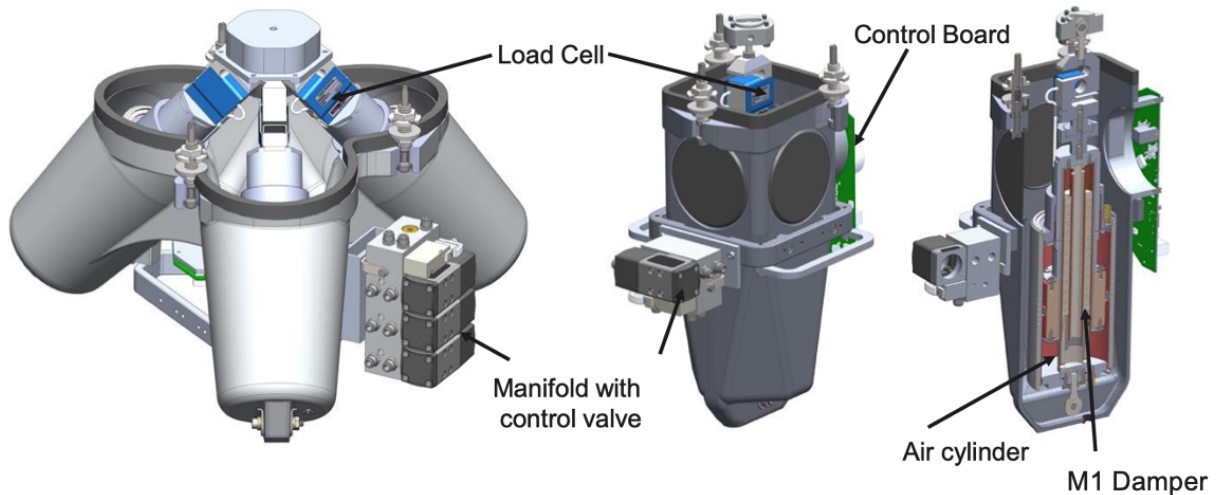


Figure 4. The design of the pneumatic support actuator. (Left) A triple-axis support actuator. (Middle) A single-axis support actuator. (Right) Cross section of a support actuator, including an eddy current damper.

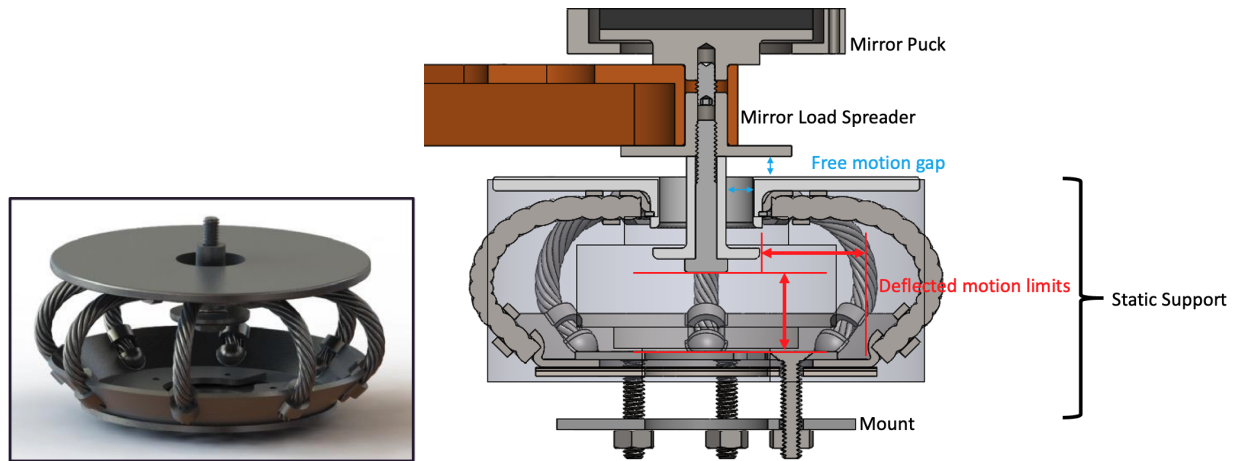


Figure 5. Static support design.

The performance of the support system is a direct function of the systems dynamic properties. Currently, each static support has an axial stiffness of about 250 N/um and a lateral stiffness of about 125 N/um. This results in piston, lateral, and tip tilt modal frequencies that are at 11.5 Hz, 8.1 Hz and 9.5 Hz respectively (there is also a twist mode, but it is less critical). The static support damping at large deflections is assumed to be 7%, but is in fact somewhat nonlinear. The resulting damping for the three modes is shown in Table 1. The damping is only shown up to 2000 Ns/m, because any more damping results in excessive force applied to the glass. 30% damping is considered the point of diminishing returns with respect to reducing seismic motion, and is never reached for the lateral modes. Thus, a target damping of 2000 Ns/m has been set.

3.3 Seismic Isolation System

The GMT features a two-dimensional seismic isolation system (SIS) that consists of a set of 24 single friction pendulum bearings located at the base of the concrete telescope pier (see Figure 1).⁵ The SIS may also include a set of viscous dampers to limit displacements, depending on the measured friction properties of the production bearings.

The single friction pendulum bearing, which is illustrated in Figure 6, consists of an articulated slider that

Table 1. Relationship Between Modal Damping (% of Critical) and M1 Damper Damping.

Damping per M1 Damper (Ns/m)	0	500	1000	1500	2000
Axial Modal damping	7%	12%	17%	23%	28%
Lateral Modal Damping	7%	9%	10%	12%	14%
Tip/Tilt Modal Damping	7%	15%	22%	30%	38%

may move along a concave stainless steel spherical surface. The friction developed between the sliding surfaces is controlled by a low-friction liner, which is selected based on the desired load and friction characteristics. If the static friction is too low, the SIS may activate too frequently. If the dynamic friction is too high, the bearings are ineffective at attenuating ground acceleration. Additionally, the motion must be smooth, with no evidence of stick-slip behavior. A similar liner material is also used to ensure smooth articulation of the slider. The initial dynamic coefficient of friction is about 0.1, and decreases to about 0.4 as the liner material grows hotter, as the bearings dissipate energy.

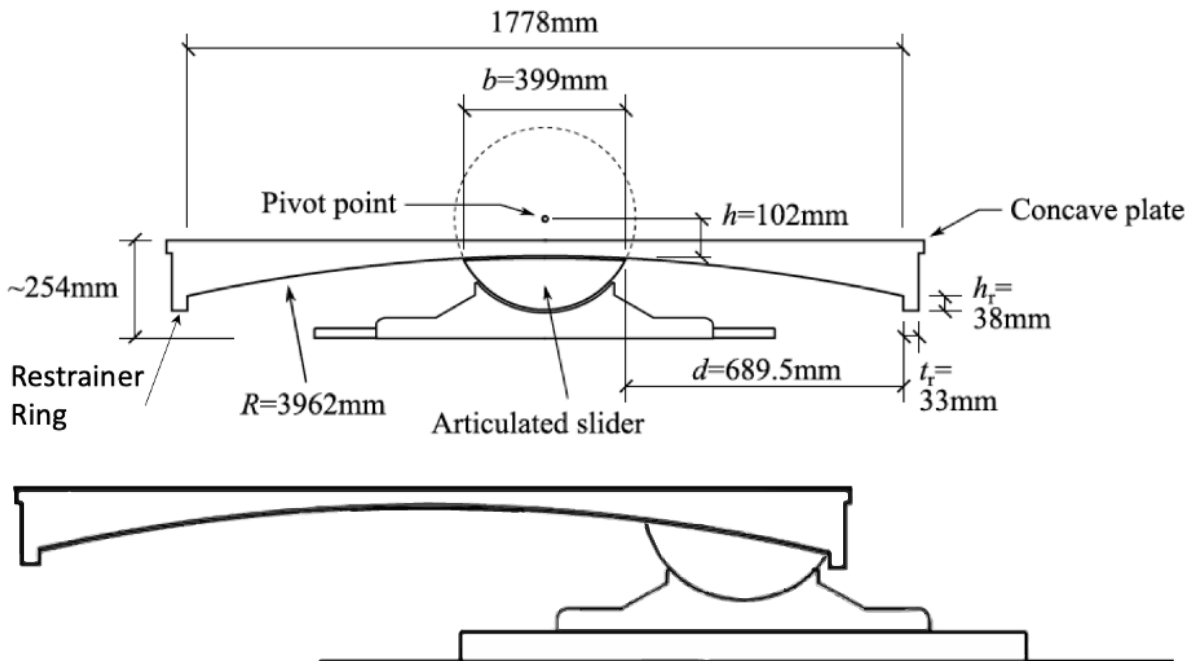


Figure 6. (Top) Design of a single friction pendulum bearing (there are 24 of these in the telescope design). (Bottom) Diagram of bearing when it is displaced to its full capacity (d).

The concave surface results in a pendulum-like motion, and thus a mass-independent natural period. For the GMT, the effective radius is approximately 4-meters, which corresponds to a natural period of 4-seconds. Thus, ground motion with a period significantly shorter than 4 seconds is decoupled, as long as the amplitude is sufficient to overcome the friction.

While the bearings are designed to accommodate more than 890mm of radial displacement, a restrainer ring is contacted at a displacement radius of 690mm. The restrainer ring is designed to fracture, consuming energy as it does so. GMTO considers bearing displacement in excess of 690mm to be a failure of the bearing because the impulse that results from restrainer ring contact is considered unacceptable.

The decision to include seismic isolation resulted from an evolved understanding of the seismic environment along with a better understanding of the corresponding telescope response, particularly at the primary mirror

segments. The friction pendulum was selected over lead-rubber bearings out of concerns for longevity and operational stiffness. Single-fiction pendulum bearings were selected over higher-order bearings out of stiffness concerns and for a desire for a deterministic, repeatable system.

4. SEISMIC MODELING

Detailed analyses are required in order to refine the design consistent with the system level requirements. The critical results for developing requirements include seismic isolator relative displacement, static support displacement, mirror stress and payload accelerations. This section includes a detailed discussion of the tools used to determine these results. The results are discussed in Section 5.

The general flow of the process used is shown in Figure 7. End products of analyses are identified in green, whereas important intermediate results are in red. Ground motions are the input to all seismic analyses and are described in Section 4.1. The seismic isolation system is modeled as a filter that takes the ground motions as inputs and outputs the motion of the base of the pier (Section 4.2). That motion is then used as input to a coupled model that includes the dynamics of the telescope, primary mirrors segments and the nonlinear elements of the M1 support system (Section 4.3). The force into the glass is then converted into stress in the mirror segments as a function of time (Section 4.4). That mirror stress can be converted into an equivalent time at a reference stress, which is then used in the calculation of failure statistics. Section 4.5 then describes how the critical outputs are used in the probability of failure estimates. The hazard curve gives the probability distribution of the ground motion, which is critical in these estimations. The effective stress safety factor is used so that the results of the probabilistic analysis can be compared to the legacy stress limit . Uncertainty is a consideration in all of the models and is used to determine a confidence bound on probabilistic results (Section 4.6).

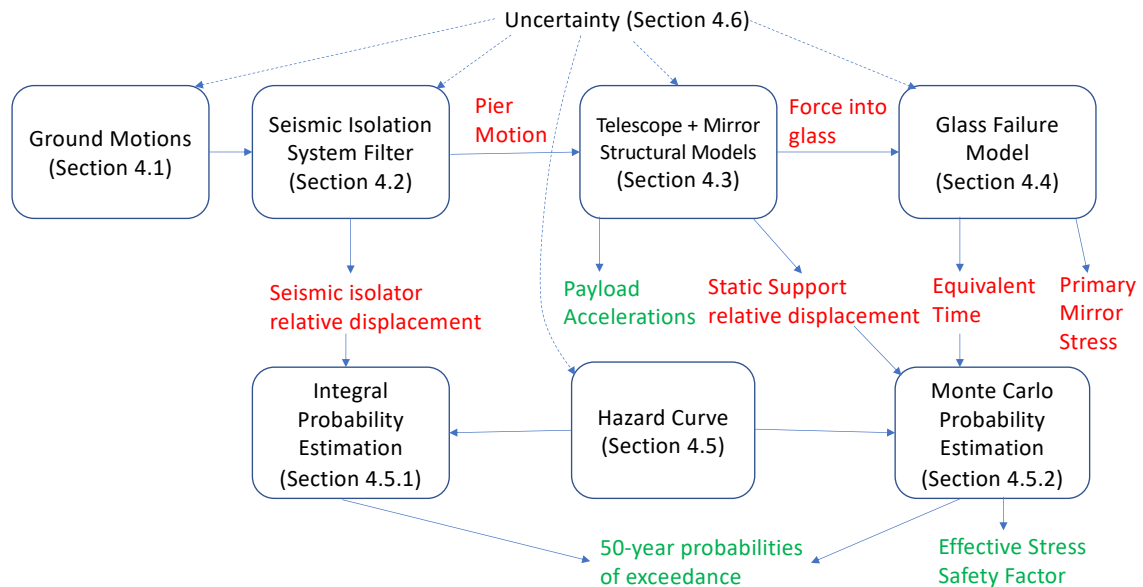


Figure 7. Flow chart of seismic modeling and analysis. End products of analyses are identified in green, whereas important intermediate results are in red.

4.1 Ground Motions

A characterization of the ground motion is necessary to perform any of the seismic analyses on the telescope, and is required by the building code. GMTO uses time series of the ground motion to perform the evaluations in this paper. One set is used to determine payload acceleration environments at discrete levels and another to determine probabilistic results for the seismic isolation system and the primary mirror segments.

A study, called a site-specific probabilistic seismic hazard assessment, has been completed to determine appropriate loading for the three different seismic levels.⁶ While these studies are standard for construction projects, this study was developed to meet the specific needs of the telescope. The assessment requires combining information about the geology and plate tectonics of the site, known ground motion records of similar locations, and various ground motion propagation models to calculate the statistics for spectral acceleration at a range of periods for the site (See Appendix A for an explanation of spectral accelerations). A simple example of the result is the peak ground acceleration for various levels of earthquake given in Table 2. More complicated results including the Uniform Hazard Spectra, adjusted Conditional Mean Spectra and Conditional Spectra are discussed below.

Table 2. Peak Ground Acceleration (PGA) at various earthquake levels

	Return Period (years)	Horizontal PGA (g)	Vertical PGA (g)
Rigidity Level	2	0.022	0.015
Operational Level	100	0.198	0.138
Survival Level	2475	0.688	0.482

The horizontal Uniform Hazard Spectrum (UHS) at the survival level is shown for 5% damping in the left hand side of Figure 8. At each period on the x-axis of the UHS, the spectral acceleration given on the y-axis is exceeded with a frequency given by the inverse of the survival level return period. This is considered a "mean spectra" meaning that several ground motion propagation models are used to determine the uniform hazard, and the resulting UHS is a weighted average of the results of those models.

The UHS has been found to be generally overconservative, and a conditional mean spectra approach has been favored in recent years. Two adjusted horizontal Conditional Mean Spectra (CMS) are also shown on the plot in Figure 8. The adjusted CMS is similar to the UHS. At the conditioning period, the UHS and the adjusted CMS are equal. The accelerations defined at other periods are the mean of the spectral accelerations expected for earthquakes that match the UHS at the conditioning period. Thus, the adjusted CMS is considered less conservative than the UHS, but closer to actual earthquake spectra making it more realistic. Note that the developed adjusted CMS match the UHS below the conditioning period for short period adjusted CMS and match above the conditioning period for long period adjusted CMS. The adjusted CMS are developed for two conditioning periods, 0.3 seconds and 2 seconds. The 0.3 second period was chosen because it is closest to the first flexible modal period of the telescope. The 2 second period was chosen because it is closest to the pendulum frequency associated with seismic isolators, and thus most likely to cause the seismic isolators to exceed their range of motion.

The corresponding vertical spectra to the UHS and adjusted CMS are also shown in the figure. The hazard analysis determined an approximate ratio between horizontal and vertical at each frequency. The same ratio is used for each spectrum. Notably the vertical spectra are very close in magnitude to the horizontal at the excitation frequencies for the primary mirrors between 8 and 12 Hz.

For analyses performed at discrete levels, ground motion time series' with a spectral acceleration matching the adjusted CMS at all periods are used. One set of seven has been developed for shorter periods and another set of seven for longer periods for operational and survival levels of earthquake. Each time series is the result of adding wavelets to measured ground motions from past earthquakes to get the spectra to match the adjusted CMS.

In order to complete a non biased probabilistic risk analysis, it is preferred that the ground motions do not include the excess conservatism found in the adjusted CMS. Conditional Spectra (CS) have been developed that remove the excess conservatism. The CS includes a CMS that is not adjusted, meaning the spectral accelerations at all periods are the mean of the spectral accelerations expected for earthquakes that match the UHS at the conditioning period. The CS also includes the lognormal standard deviation of the results at each period. One example set is shown on the right side of Figure 8. These were developed along with 16 acceleration time series

that were chosen so that their spectral variation approximately adhere to the CS (shown in black). Again, the spectra and time series were developed at the operational level and survival level, and conditioned at short and long periods. These provide an unbiased description of the hazard and are useful for more precise methods of risk analysis discussed later.

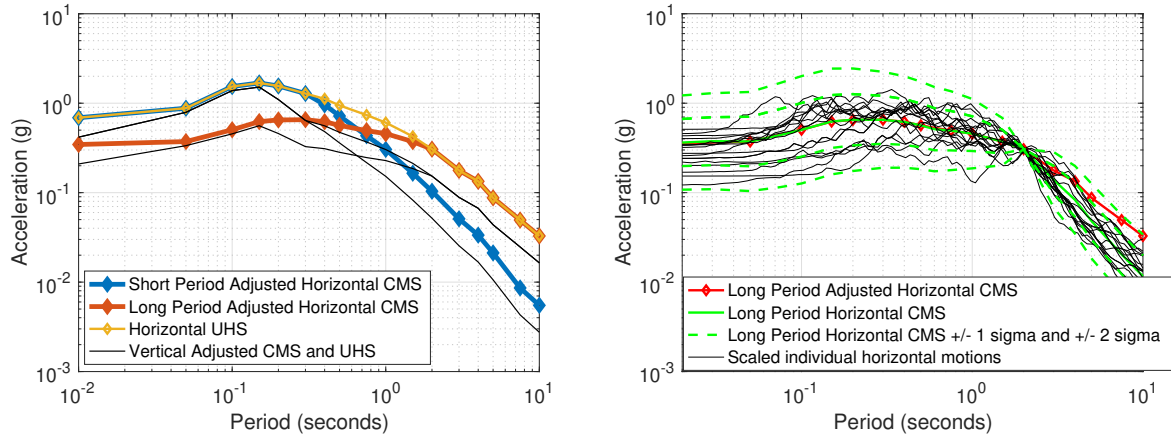


Figure 8. (Left) 5% damped response spectra for survival level adjusted CMS and UHS. (Right) 5% damped response spectra for survival level long period conditional spectra, along with the 16 spectra of the selected (and scaled) ground motions and the adjusted long period CMS.

4.2 Seismic Isolation System Filter

The seismic isolation system is the only connection between the telescope pier and the ground. Thus, models of the seismic isolation system are needed for any dynamic analysis of the telescope, and to evaluate the survival of the seismic isolators themselves.

For seismic analyses the entire seismic isolation system is modeled in MATLAB with a simple nonlinear ordinary differential equation for its active motion.⁷ These equations act as a filter, taking the input 3 degree of freedom time series with 2 horizontal and one vertical degree of freedom, and outputting the filtered 3 degree of freedom time series. As a simplification of the dynamics, the output vertical motion is equal to the input. The vertical ground motion does effect the horizontal response, however, adding to the normal force.

When the differential equation is simplified to one degree of freedom the resulting filter is

$$\ddot{x} = -a_x(t) - \frac{g}{R_e} \left(1 + \frac{a_z(t)}{g}\right)x - \mu g \left(1 + \frac{a_z(t)}{g}\right)h - b\dot{x} \quad (1)$$

$$\dot{h} = \frac{1}{Y} \left(\dot{x} - \frac{1}{2}|h\dot{x}|h - \frac{1}{2}\dot{x}h^2\right) \quad (2)$$

where the inputs are horizontal and vertical ground motions, $a_x(t)$ and $a_z(t)$, and the output is the relative displacement across the isolation system, $x(t)$. The acceleration of the base of the pier is another important output and is calculated as $\ddot{x} + a_x$. h is a hysteresis term that smoothly deals with the transition to sliding. R_e is the radius of curvature of the isolator (approximately 4 meters). b is the viscous damping coefficient, divided by the mass above the isolators. μ is the dynamic coefficient of friction, g is the acceleration of gravity, and Y is the yield displacement (the displacement when sliding begins, which is inversely proportional to the isolation system lateral stiffness). The $\frac{g}{R_e} \left(1 + \frac{a_z(t)}{g}\right)x$ term is responsible for the pendulum motion. The $\mu g \left(1 + \frac{a_z(t)}{g}\right)h$ term represents the friction force when the isolator is sliding (and $|h|$ is close to 1), and the stiffness of the isolator when the isolator is not sliding (and $|h|$ is small).

The dynamic friction in the model can vary with pressure, temperature and velocity, but those relationships are not shown here. The friction goes up with velocity and down as the mass above the isolator increases, but

neither effect is significant. The temperature relationship, however, is critical. As the isolator heats up from the friction, the friction coefficient drops, reducing the friction by as much as 60%.

Though the two most important outputs of the model are the acceleration of the base of the pier, and the relative displacement between the two side of the isolation system. It is also important to consider the failure due to wear. This can be done by calculating the energy dissipated by friction during a response (which is not further discussed in this paper).

An example of the response to a short period survival level earthquake is shown Figure 9 in both the time domain and frequency domain. The red represents input ground motions and the blue represents the output. Note in the time domain that the response is limited to about 0.1g. This exemplifies that the horizontal acceleration is limited to about μg (and in this case μ is 0.08). The frequency domain plot demonstrates that the reduction in the spectral acceleration is inversely related to the period. The spectrum is reduced by as much a factor of 5 at short periods, but closer to 3 at the large modal mass frequencies of the telescope (3-5 Hz). Recall, the seismic isolation system does nothing to isolate the vertical motion. After the application of seismic isolation the motion of the base of the pier is dominated by the vertical term.

Two sets of relative displacement responses to long period survival level earthquakes are shown in Figure 10. This is important to assess the risk of exceeding the total displacement capacity of about 700mm. While both are considered survival level events based on their return period, one takes up more than 3 times the displacement. This demonstrates a few key points. First of all, the cost of the low friction that lowers the horizontal accelerations into the telescope is that there is higher risk of exceeding the isolators' displacement capacity. The curvature of the bearing is meant to supply a return force, but cannot be increased enough to significantly mitigate that risk. Also, by choosing earthquakes based on 5% damped spectral acceleration (as is the norm in hazard assessments), the relative displacement responses in the set vary widely. If the hazard assessment would have been performed using spectral displacements the set would be more consistent, and exhibit less uncertainty. On the right hand plot, viscous dampers have been added at a level of 50% of the critical for the pendulum mode. This reduces the relative displacement by about 50%.

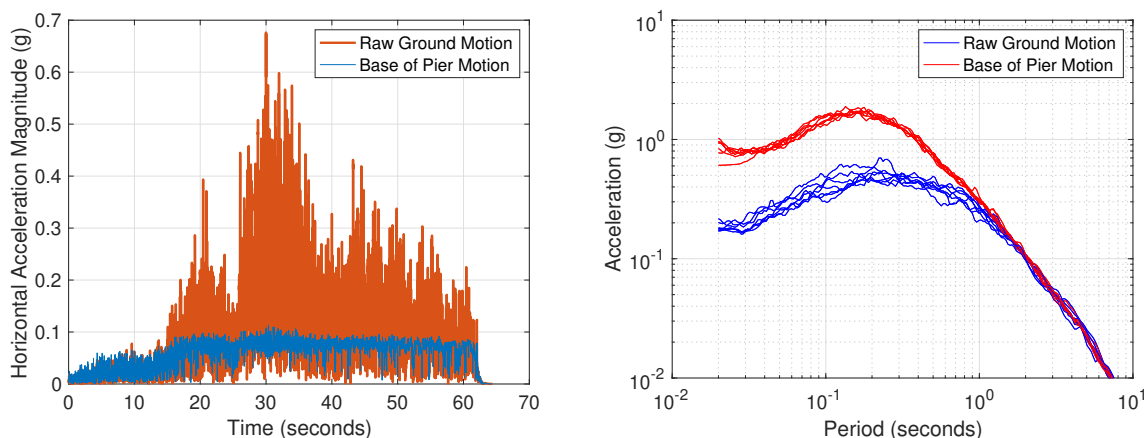


Figure 9. A comparison of ground acceleration to the acceleration of the base of the pier when supported by seismic isolators. (Left) A single time series. (Right) Spectral accelerations associated with the 7 adjusted CMS time series.

4.3 GMT Seismic Tool

GMTO has developed a MATLAB tool to efficiently simulate the response of the telescope and primary mirrors to seismic loads at the above the seismic isolation system, called the GMT Seismic Tool. The tool includes reduced order models of the pier, telescope and primary mirrors, and includes nonlinear elements at key interfaces. A schematic of the tool is shown in Figure 11. An important feature of the model is that it is built in a parametric way, so that key properties and configurations can easily be adjusted, facilitating trade studies. The approach is similar to that used by GMTO to analyze the tracking jitter in response to wind.^{8,9}

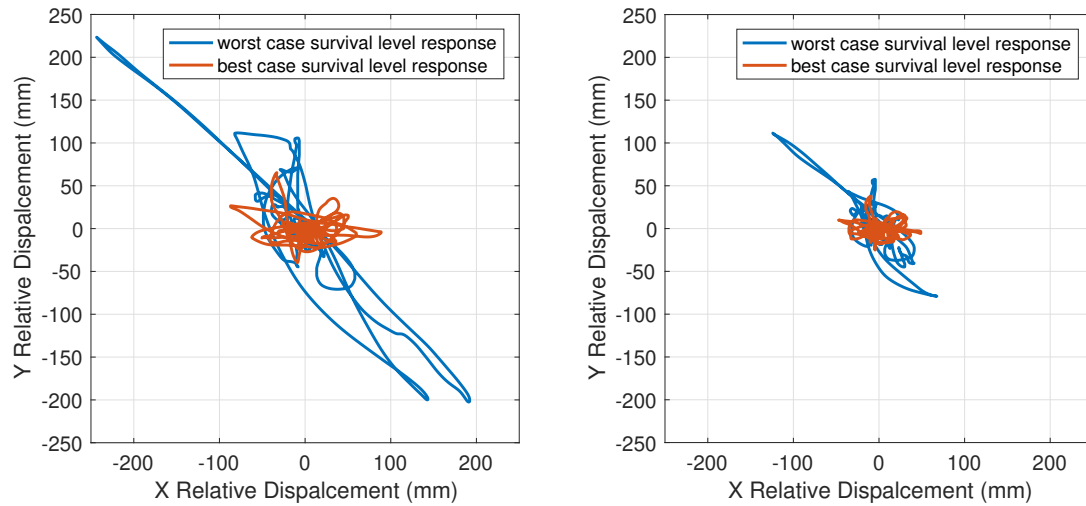


Figure 10. (Left) Relative displacement between two sides of the seismic isolator in response to two different survival level events. (Left) Without additional viscous damping. (Right) With additional viscous damping.

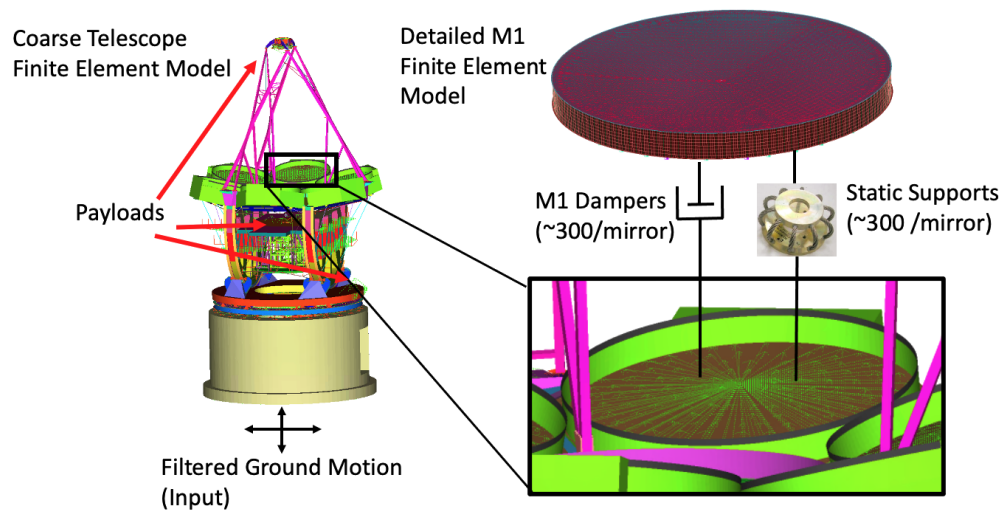


Figure 11. The Giant Magellan Telescope Seismic Tool.

The telescope and pier finite element model has a medium to coarse mesh, and includes mostly plate elements and some beams. Most payloads are modeled only as a point mass. The results are very sensitive to the modal damping selected for this part of the modal. While steel structures like the mount can have modal damping as low as 0.25% for small motions, large motions have more damping. The manufacturer of the mount has advised that 2% damping is a reasonable amount to use, and that is what is used for system level analysis.

The primary mirror and its support system are modeled in detail. A separate reduced order finite element model is used for the mirror, since its mesh is much more refined than that of the telescope. It is also modeled with plates, and the hexagonal cells used to lightweight the mirror are explicitly modeled. Forces are applied at the centers of the loadspreaders. The telescope finite element model has interfaces at the same locations, so that the resulting reduced order models can be interfaced.

In the current model the only nonlinear feature modeled is the nature of the gaps in the static supports. Each static support applies no force while loadspreader is in the gap and applies linearly varying force beyond

the gap. An example of the axial gap is given in the equation

$$F = -k \left(x - \frac{x}{|x|} gap \right) \quad \text{for } |x| < gap \quad (3)$$

$$0 \quad \text{otherwise.} \quad (4)$$

The axial gap is +/- 6mm while the radial gap is 8mm. That means that the mirror can move freely in a cylinder with a 8mm radius and 12mm length. There are approximately 3 static supports per load spreader. Thus in the model the stiffnesses are scaled accordingly.

The only part of the support actuators that is modeled is the damping provided by the M1 Dampers. Each M1 Damper applies a force proportional to velocity. Because of the orientation of the support actuators, there is significantly more damping in direction normal to the backplate of the mirror than in the plane of the backplate.

The structural modeling includes a number of simplifications. The behavior at the limits of the static support stroke is not modelled and instead the exceedance of the range of motion is simply considered a failure. There are also significant nonlinearities in the static supports not currently modeled. Finally, the hydrostatic bearings at the base of the mount can lift off the telescope in reality, but not in the model. This is feature that is planned to added later, though the current model outputs can be used to determine IF uplift would occur.

The key outputs of the tool include time histories of the primary mirror interface forces, primary mirror interface displacements and accelerations of all payloads. The primary mirror interface forces and displacements are used to determine the failure of the primary mirrors, and the payload accelerations are used to develop requirements for all other payloads.

4.4 Glass Stress and Failure Model

The primary mirror glass has two direct failure modes considered in the analysis. The first, as discussed in the previous section, is exceeding the range of motion of the static supports. The second is a failure due to cracks caused by repetitive stress in the glass. In order to calculate this failure, the principal tensile stress is broken into annealing, thermal and mechanical stress. In this analysis the annealing stress is assumed to be a constant 0.7 MPa. The thermal stress, developed by non uniform coefficient of thermal expansion and temperature distributions, is also assumed to be a constant 0.7 MPa. The remaining portion is the mechanical principal stress, and includes contributions from constant gravity loading as well transient events including seismic and transport loads.

The mechanical principal stress is the component of stress in response to the external forces applied to the glass. It is determined using the output of the GMT seismic tool and is itself broken into two components, local and global stress. The local stress is the stress developed close to the location of supporting forces. It is calculated by multiplying the stress by scale factors that were determined using a more detailed finite element model. The global stress is calculated using a static reduction of the same plate mesh of the primary mirror that is used in the GMT seismic tool. Stress close to the pucks are ignored in the global stress. There are a variety of ways to sum global and local stress of varying degrees of conservatism.

Local witness samples of the glass were tested to find the statistics for failure in the glass. The statistics have been fit to a Weibull statistical model for failure. The Weibull statistical model determines a probability of crack formation based on full time history of the stress. A version of that statistical model is given in Equations 5 and 6. Different portions of the glass have different failure statistics, due to the different quality of surface finish. The polished surfaces are the least likely to form cracks.

Typically this model is used to justify limits for the peak stress by applying that peak stress as a constant stress over a given time. For example, 1 hour at 5.0 MPa has a 1.0% probability of failure for areas with the roughest surface finish. This can be loosely related to the peak glass stress limit for short duration mechanical stress of 1.0 MPa by choosing safety factors to apply to each stress component. An appropriate set of safety factors for short duration stress is 2.0 for thermal and annealing stress and 2.2 for mechanical stress. This method, however, clearly adds conservatism. The stress is close to the peak for only a few seconds during any seismic event, yet the one hour limit is used. When it proved difficult to economically reduce the stress below

this limit, the decision was made to pursue method that took advantage of the inherent probabilistic nature of the Weibull model.

In order to utilize the Weibull statistics in a probabilistic analysis it is convenient to introduce the concept of equivalent time. Any stress time history can be converted into an equivalent time at a given reference stress. The time histories are equivalent in that they both have reached the same accumulated probability of crack formation. Equivalent times from various seismic events can be summed together, and the total equivalent time can be found. Finally, the total equivalent time can be converted to a probability of crack formation. The process is given by the equations

$$\epsilon_i = (t_i - t_{i-1}) \left(\frac{S_i}{S_r} \right)^n \quad (5)$$

$f = 1 - e^{-(K S_r \sum_i \epsilon_i)^\beta}$ (6) where t_i and S_i are the time and stress at time step i , ϵ_i is the equivalent time at reference stress S_r at time step i , K and β are constants associated with the Weibull distribution, and f is the probability of crack propagation. The examples given in Figure 12, demonstrate how failure varies with time, stress and surface finish.

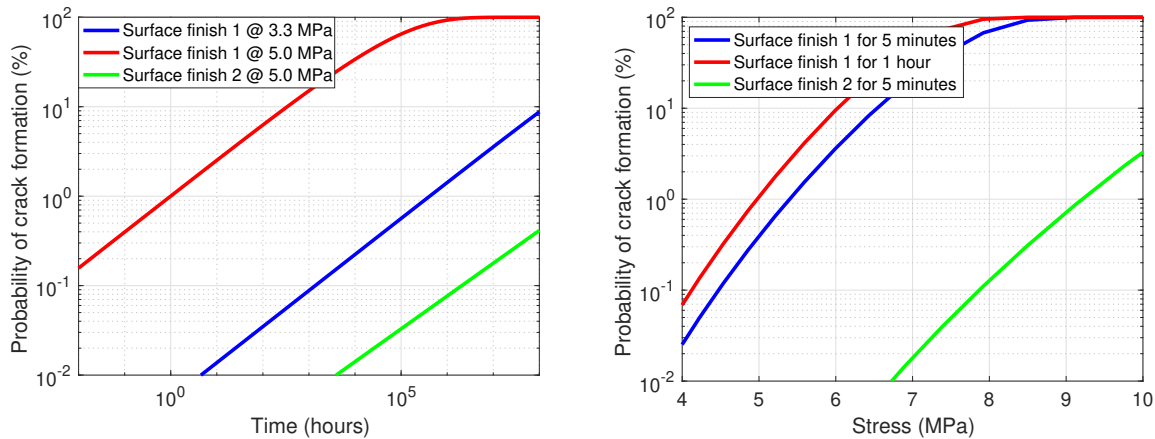


Figure 12. Examples of the Weibull probability of failure model.

4.5 Probability of Failure Estimation

There are two methods used to determine the probability of a given event occurring on the telescope, the integration method and Monte Carlo method.* The integration method is a little more straightforward and is the more common approach. The method unfortunately cannot be used for cumulative failure, which necessitates a Monte Carlo approach.

Both methods require the probability distribution of the input ground motion. This is given by the hazard curve determined as part of the site-specific seismic hazard analysis. The hazard curve plots the annual frequency of exceedance of a certain parameter against the value of that parameter, as shown in left hand side of Figure 13. The parameter can be peak ground acceleration, or the spectral acceleration for a given frequency and damping. The probability distribution function, λ , is calculated from the hazard curve by taking the derivative as in the equation

$$\lambda = - \frac{dAFE(Sa)}{d(Sa)} \quad (7)$$

*The combination of various analyzed probabilities of failure are not covered in this paper, and the determination of uncertainty bounds is covered in the next section.

where $AFE(Sa)$ the annual frequency of exceedance as a function of spectral acceleration Sa . Notably, the annual frequency of exceedance is the inverse of the return period. The frequency f (in units of average number of events per year) of an earthquake in a given range (from Sa_1 to Sa_2) is computed in the equation

$$f(Sa_1 < Sa < Sa_2) = \int_{Sa_1}^{Sa_2} \lambda dSa = - \int_{Sa_1}^{Sa_2} dAFE(Sa). \quad (8)$$

Both methods also require that simulations be performed at various seismic levels, besides the ones which time series were explicitly provided. Above the survival level earthquakes, the survival level earthquake can simply be scaled according to the hazard curve. Between the operational level earthquake and the survival level earthquake time series from both can be scaled by the hazard curve, and any resulting performance results combined in a weighted average. The weighting is informed by the 500 year, 1000 year and 1500 year return period spectral accelerations, also provided as part of the site-specific seismic hazard analysis.

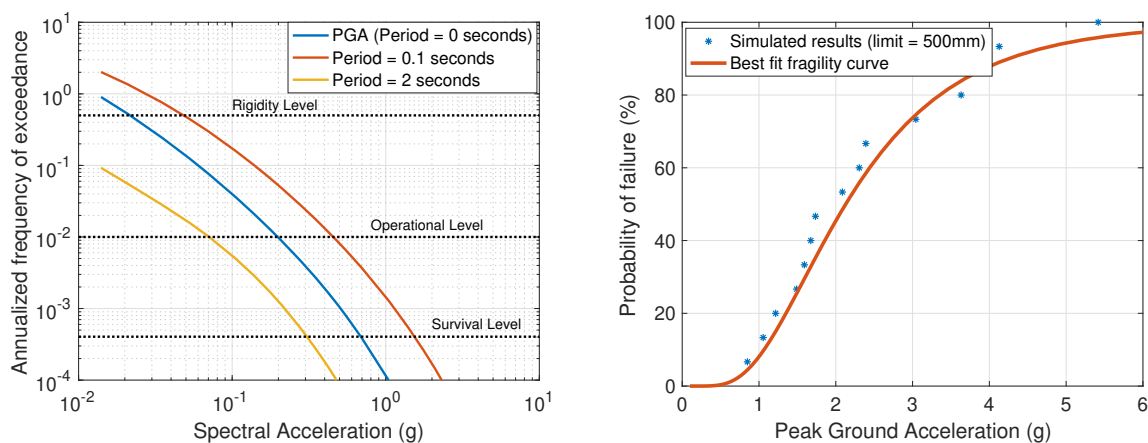


Figure 13. (Left) Mean hazard curves for the GMT. (Right) Example of fragility curve for seismic isolator relative displacement.

4.5.1 Integral Method

In order to use the integration method it is necessary to first determine a fragility curve. An example is given on the right hand side of Figure 13. In order to determine the fragility curve for a given quantity, for example seismic isolator displacement, a threshold, called a limit state, is given. Each point on the fragility curve is the probability of exceeding that limit state, given a certain spectral acceleration or peak ground acceleration. Thus, an individual point on the fragility curve is the weighted sum of 100's for every scaled time series that results in an exceedance of the limit state and 0's for every scaled time series that does not. These are represented symbolically as $p(Sa, ls)$ where the limit state is represented as ls (for limit state). These fragility curves are integrated by the conditional probabilities in the hazard curve at each earthquake level, to determine the probability of exceeding any given limit state ($poe(ls)$), as demonstrated in the equation

$$poe(ls) = \int_0^{\infty} p(Sa, ls) \lambda(Sa) dSa = - \int_0^{\infty} p(Sa, ls) dAFE(Sa). \quad (9)$$

An example result is described in Section 5.3.

4.5.2 Monte Carlo Method

Unfortunately, the integral method does not apply to cumulative equivalent time. The integral approach depends on events being independent, but, as discussed in the previous section, the probability of failure of the glass depends the entire stress history of the glass. Thus, a Monte Carlo method is used to determine the probability of glass failure. The key to the implementation of this method is that the year in which an earthquake occurs is

taken as a continuous variable while the intensity is discretized into bins. This allows for multiple earthquakes to occur during any given time period. The process has been validated against the integral method.

First, a statistical model of some performance metric, pm , is made as a function of return period. Thus $p_{rp}(pm)$ is the probability density function (PDF) for that performance metric, for a given return period. Individual PDF's can be created using a Monte Carlo approach at discrete return periods (alternatively the Latin Hypercube approach is proposed to be more efficient). Then the distribution at any return period can be determined through interpolation. An example is given on the left hand plot Figure 14.

Next a sequence of earthquake return periods are randomly distributed across $50 * NL$ years, where NL is the number of 50 year observatory lifetimes in the study. The level of the earthquake is simply recorded as the "return period" assigned to that earthquake. An example is given as the right hand plot in Figure 14. Note that over 500 years, earthquakes with greater than or equal to 100 year return periods are expected to occur 5 times, and in this example, they do.

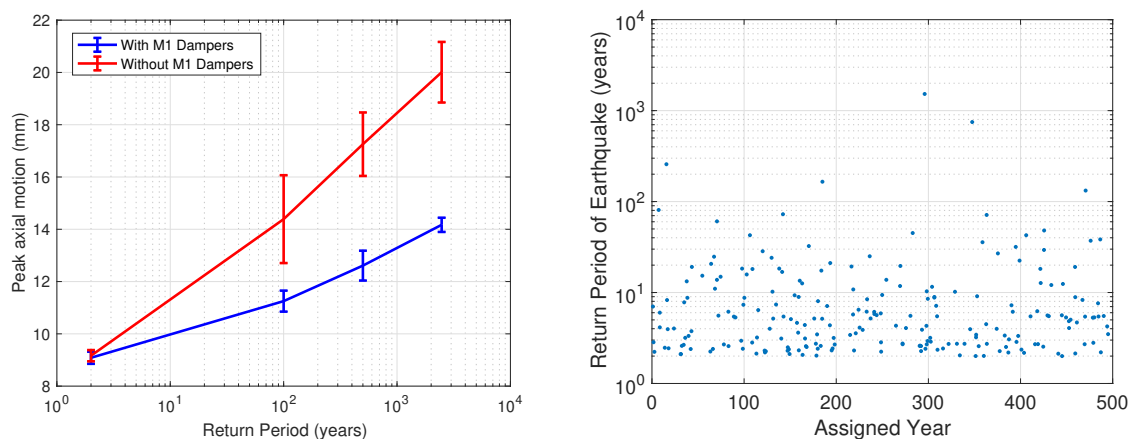


Figure 14. (Left) Probability distribution function of the peak axial motion of any static support against return period. The midline is the mean and the errorbars are the standard deviation. (Right) Snapshot of simulated earthquakes in a Monte Carlo simulation.

Next, return period is mapped to spectral acceleration through the hazard curve. Then, the performance metric is randomly assigned for each earthquake by using the probability density function for the spectral acceleration of each earthquake. In the last step, the maximum of each performance metric in each 50 year time period is taken. In the case of equivalent time, the sum of the equivalent times is taken (added to the 50 year baseline stress equivalent time). With enough 50 years time periods a probability distribution can be attained as shown in Figure 16.

4.6 The Role of Uncertainty

An accurate probabilistic analysis relies heavily on a characterization of the underlying uncertainty. Typically uncertainties are divided into two types, aleatoric and epistemic. The aleatoric uncertainty refers to the randomness from event to event. The epistemic uncertainty refers to uncertainty in knowledge of the aleatoric uncertainty. For example, one might predict a coin flip to be heads fifty percent of the time. That is an example aleatoric uncertainty. But one does not know if the coin is somehow biased. That lack of knowledge is an example epistemic uncertainty.

The methods discussed in the previous chapter can be used to predict a single, unbiased, probability of failure for the telescope using only aleatoric terms. In order for the probability to be unbiased, the models are built using predicted (not conservative) properties. By adding the epistemic terms, we can instead describe the range of possible probabilities of failure (also called a confidence interval).

The driving aleatoric terms are the intensity of seismic event at the site, the specific earthquake signal chosen, the telescope azimuth angle and the telescope zenith angle. These are assumed random in the derivation of the mean statistical model for a given failure metric.

The epistemic terms are countless, though aspects are measurable. For example, in the site-specific seismic hazard analysis, several ground motion prediction equations are used, and the given spectra are based on a weighted mean of the results of those models. The analyst also randomizes the weightings to produce a probability distribution of the spectra at each return period. The results, called fractiles, include spectra at the 85th percentile (about one standard deviation above the mean). At the survival level, this is about 20% larger than the provided mean. In the analysis of the seismic isolation system displacement, the fact that 5% damped spectral acceleration poorly correlates with the relative displacement introduces additional epistemic uncertainty, because the given time series may not provide a suitable sample with which to form statistics.

In the seismic isolator, telescope, and mirror models, every unknown property, simplification, assumption or error produces epistemic uncertainty. The differences from analyst to analyst is yet another source of uncertainty. Sensitivity analyses are done to characterize as many of these terms as possible, which is one of the advantages of the tools GMTO uses. Ultimately, the epistemic uncertainty in the ground motion, the telescope damping, and nonlinearities in the static supports contribute the most to epistemic uncertainty.

Ideally the epistemic uncertainty in the GMT results can be characterized by applying a statistical model to certain parameters to determine a statistical distribution of the failure metric (this is the method used by the ground motion analyst). For now, assumed standard deviations are combined with a root-sum-squared approach. An example of how the results are used appears in Figures 16 and 9.

5. PRELIMINARY RESULTS

5.1 Primary Mirror Stress

The results of an early study to demonstrate the effectiveness of the seismic isolation system and the M1 Dampers is shown in Figure 15. For this study, the seismic isolation system filter and the GMT seismic tool were used to determine the mirror stress for the earthquakes at the 3 given seismic levels. The model was run with and without seismic isolation, and with and without additional damping in the M1 support system. The midline is the mean of the results, and the errorbars are the standard deviation of the results. The seismic isolation system has a small effect for the smaller earthquakes, but has a dramatic effect for larger earthquakes. The M1 Dampers, as expected by their linear nature, cause a more consistent reduction in stress. The two effects combined reduce the mechanical stress by more than a factor of 3. But the stress is still larger than the 1.0 MPa limit. Thus, in order to demonstrate the likelihood of compliance, the probabilistic approach is needed.

In order to evaluate failure in probabilistic terms, the Monte Carlo method was used. For each earthquake, the mechanical stress at each time step must be added to the thermal and annealing stress as shown in the equation

$$S_i = S_{thermal} + S_{annealing} + S_{mechanical,i} \quad (10)$$

where $S_{thermal}$ is 0.7 MPa and $S_{annealing}$ is 0.7 MPa. For each 50 year period, the equivalent time from multiple earthquakes is added to the equivalent time from 50 years at static gravitational loads. When this process is done, the probability of failure is less than 0.01%. In order to get a sensible result, it was required to add the notion of a safety factor. Thus, the stress at any time stamp i is computed by the equation

$$S_i = SF_{thermal} * S_{thermal} + SF_{annealing} * S_{annealing} + SF_{mechanical} * S_{mechanical,i}. \quad (11)$$

The equivalent safety factor can be found by increasing the mechanical safety factor until the probability of failure is 1%. When a safety factor of 2.0 is used for thermal and annealing, the resulting mechanical/seismic safety factor is 3.5 without dampers (and with seismic isolation) and 5.5 with dampers. As discussed in section 4.4, the stress safety factor associated with the glass stress limits is 2.2. Thus, the primary mirrors have been shown to effectively meet the legacy deterministic limit by having a larger safety factor using probabilistic methods.

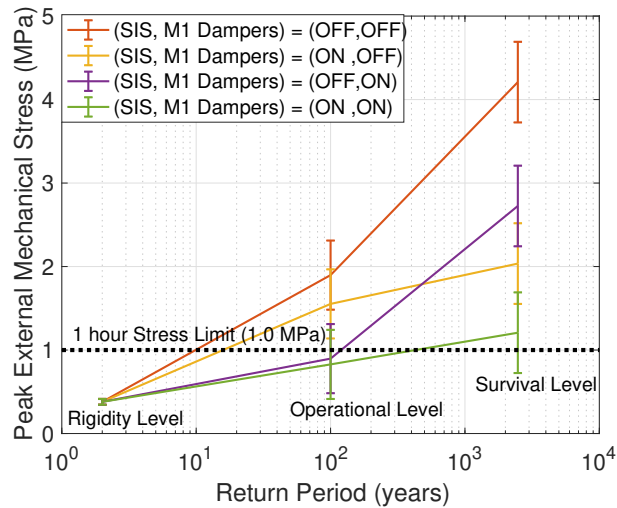


Figure 15. Comparison of stress results at various earthquake levels, demonstrating the effectiveness of the seismic isolation system (SIS) and M1 Dampers.

5.2 Static Support Displacement

A study of probability of static support exceedance of its range of motion is shown in Figure 16. It is clear that without actuator damping, the axial range of motion is expected to be exceeded about 5% of the time. When actuator damping is added a margin of almost 5 mm is achieved. The conservative end of the confidence interval is also shown, indicating that, with our current understanding of the model, the 85th percentile model would reach the axial limit with a 0.6% probability over 50 years. More studies like this one may be used to justify increasing the required stiffness of the static supports to gain some more margin with respect to static support displacement, while only modestly increasing peak stress.

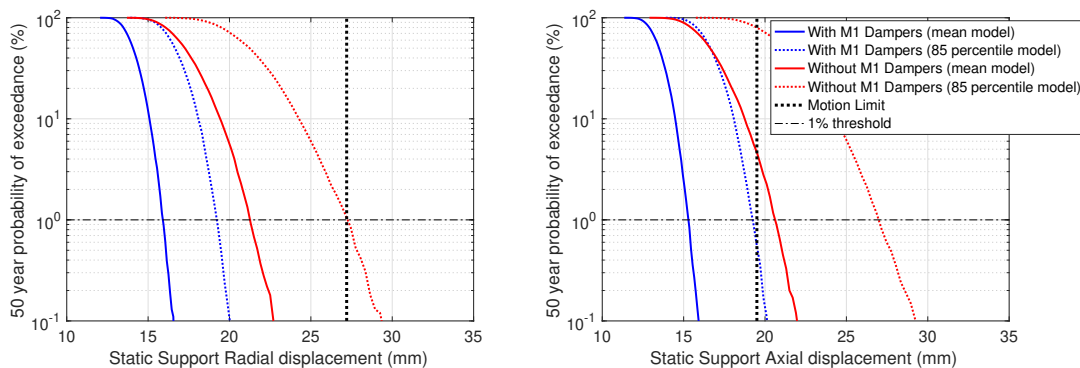


Figure 16. Mean and 85th percentile probability of exceedance curves for radial and axial static support displacement, with and without damping.

5.3 Seismic Isolation System Displacement

The seismic isolation systems main failure mode is the exceedance of its range of motion. This damages the single friction pendulum bearings, which are considered extremely difficult to replace, and causes a large and dangerous shock into the telescope. As discussed earlier, this failure mode is particularly concerning because there is a large spread of responses from earthquake to earthquake for a given return period.

The two major design features that effect the expected displacement are the dynamic coefficient of friction and externally applied viscous damping. The radius of curvature has only a limited effect. A preliminary probabilistic analysis of the effect of viscous damping is shown in Figure 17. In this case, a very small value is used for the dynamic coefficient of friction. The seismic isolation system filter is run at many different earthquake levels with two levels of externally applied viscous damping. Using the integration method, it is possible to compute the probability of exceeding various radial displacements for each case. The displacement limit in the design is about 700 mm. Thus, without viscous damping, it appears the design fails with about 0.5% probability. With 50% of critical damping applied by viscous dampers, the risk is lowered to barely 0.04%.

The project intends to use plots like these to decide whether the risk reduction by viscous dampers is worth the additional cost. Its worth noting that viscous damping does slightly increase the transmission of higher frequency ground motions into the pier, but the effect is small (on the order of 10% at the most sensitive frequencies).

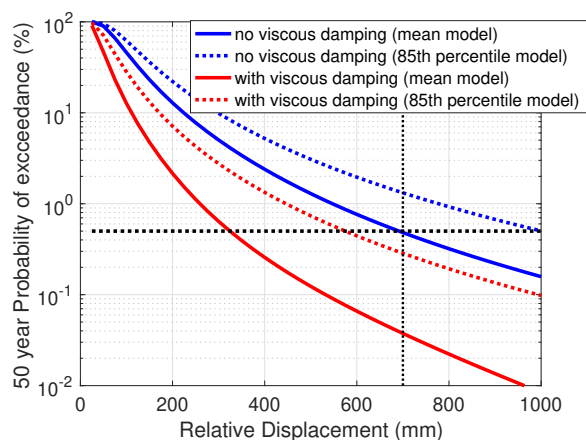


Figure 17. Example result from the seismic isolation system analysis that demonstrates compliance with the 0.5% probability of failure requirement, and modest improvement when external viscous dampers are added..

5.4 Telescope Payload Acceleration

The telescope structure hosts more than 100 individual payloads including optics, instruments and electronics cabinets. Each of these payloads must be designed for the three seismic levels. At the same time, the mount design is being refined. In the earlier stages of the project, the peak acceleration experienced at each payload location was taken from the finite element model. Then the mount was given a requirement to not exceed that acceleration, and the payload was given that as a quasi-static load. The architecture was problematic because it did not properly account for the dynamics of the payload.

The updated methodology uses response spectra as the way to communicate both the mount limit and the environment at the payloads. The mount is divided into about 20 regions. An example of one such region is shown in Figure 18. The 2% damped spectral acceleration is broken down into lateral (in the plane of the mounting interface) and normal (normal to the plane of the mounting interface). The average response spectra over the given earthquake time series for several payloads in a particular region are shown. A piecewise continuous envelope is developed to determine a "do not exceed" limit for the mount. Then limit is shifted up and the break points moved outward to include both amplitude and frequency reserve in the payload environment. If the payload is designed to be sufficiently stiff (with a lowest modal frequency above 60 Hz) the spectral acceleration limit is equivalent to a quasi-static acceleration limit, and the payload can ignore the dynamic component. If the payload is on isolators, it can determine how much load will be passed through at the isolation frequency using the spectral acceleration. And if the payload is flexible, a response spectrum analysis can be used to determine failure. This method has proven to be an efficient way to accurately communicate acceleration limits to the mount vendor and the seismic environment to the payload vendors.

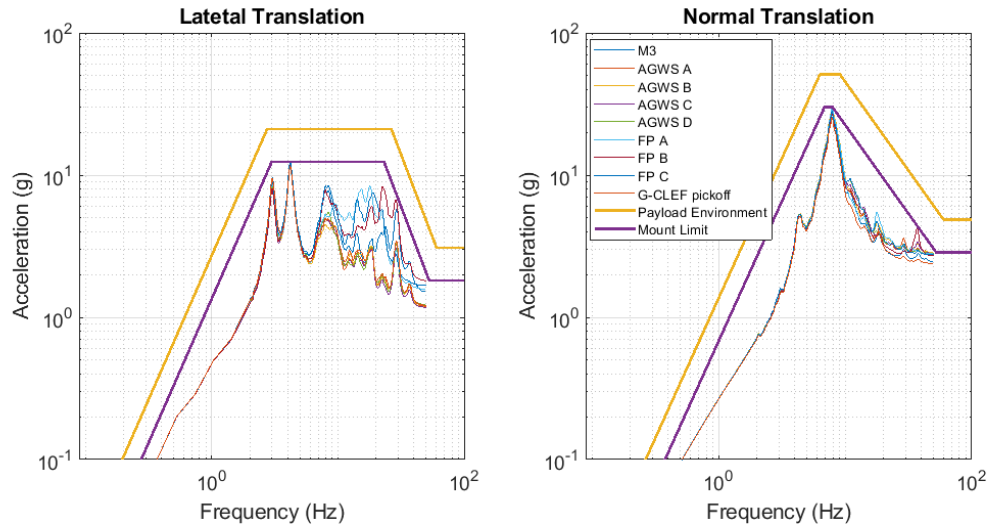


Figure 18. 2% damped spectral accelerations of the mount payloads on the instrument rotator, along with the derived "do not exceed" limit and payload environment.

6. CONCLUSION

The design architecture with single friction pendulum bearings at the base of the telescope pier and a primary mirror support system with enhanced damping has been demonstrated through detailed analysis to protect the telescope from the extreme seismic environment in Chile. Novel tools have been developed facilitate risk based decisions and can be easily updated as the design matures. The end result is that GMTO has developed a comprehensive strategy to seismic design that allows for design decisions to be made based on trade offs between costs and quantified risk.

APPENDIX A. SPECTRAL ACCELERATION

A standard tool used in seismic analysis is the spectral acceleration (also called the response spectrum). The spectral acceleration takes a time domain signal and converts it into the frequency domain. It is useful for structural design because it characterizes a theoretical peak response, which is closely correlated with structural failure. A single data point on a spectral acceleration is the response of a simple mass-spring system with a given natural frequency and damping to an input signal defining the motion at the base. The response in a single degree of freedom is computed using the equation

$$\ddot{x} = 2\zeta \frac{2\pi}{T} (\dot{x} - \dot{u}) + \left(\frac{2\pi}{T}\right)^2 (x - u) \quad (12)$$

where $u(t)$ is the base motion (and can be ground motion or any other input signal), $x(t)$ is the response motion, ζ is the percent of critical damping and T is the natural period of the mass-spring system. The spectral acceleration is $\max_t |\ddot{x}|$ and the spectral displacement is $\max_t |x|$ for a given damping and period. The spectral acceleration can also be computed for two dimensional inputs as a single acceleration vs. period relationship. One example is the RotD50 response used in the right hand plot of Figure 8. Spectral acceleration and displacement are typically plotted as a function of natural period at a given damping. The ground motion is typically described in terms of a 5% damped spectral acceleration of the ground motion. This is generally useful for civil engineers because 5% damping is close to the damping expected of most buildings. Thus, if a building has modal response dominated by a low frequency mode, one can approximate the inertial loading directly by taking the spectral acceleration at that frequency. For structures with more complicated modal response, a more complicated response spectrum analysis can be used to evaluate the design.

As the period approaches 0 seconds, the spectrum reaches an asymptote that is equal to the peak acceleration of that signal, $\max_t |u|$. For ground motion, this is called peak ground acceleration (PGA).

ACKNOWLEDGMENTS

The authors would like to acknowledge the many who have contributed to this effort, and list a few of the largest contributors in particular. Paul Blleloch and Robert Lacayo from ATA Engineering Inc. helped build the GMT Seismic Tool. Dr. Michael Constantinou provided the initial models of the seismic isolators. C.B. Crouse from AECOM developed the site-specific seismic hazard analysis. The University of Arizona Richard F. Caris Mirror Lab provided the groundwork and much of the methodology used for evaluating glass failure. Frank Kan and Mohamed Talaat of SGH helped refine the approach to seismic risk analysis. And finally Ben Irarrazaval had the original idea for the GMT seismic tool and started much of this effort.

REFERENCES

- [1] Kan, F. W. and Antebi, J., “Seismic hazard: analysis and design of large ground-based telescopes,” in [*Ground-based and Airborne Telescopes II*], Stepp, L. M. and Gilmozzi, R., eds., **7012**, 960 – 969, International Society for Optics and Photonics, SPIE (2008).
- [2] Whitby, B., “On Shaky Ground.” SPIE News, 1 May 2020 <https://spie.org/news/photonics-focus/mayjun-2020/on-shaky-ground?SS0=1>. (Accessed: 9 November 2020).
- [3] Tsang, D., Austin, G., Gedig, M., Lagally, C., Szeto, K., Sagals, G., and Stepp, L., “TMT telescope structure system: seismic analysis and design,” *Proc SPIE* (08 2008).
- [4] Marchiori, G., Rampini, F., Mian, S., Lotto, L. D., Camata, G., and Bressan, R., “ELT dome and telescope: a unique prototype in a highly seismic context,” in [*Advances in Optical and Mechanical Technologies for Telescopes and Instrumentation III*], Navarro, R. and Geyl, R., eds., **10706**, 265 – 277, International Society for Optics and Photonics, SPIE (2018).
- [5] Manuel, E. A., Constantinou, M. C., Grigel, E., Bigelow, B. C., Terán, J., and Talison, B., “Telescope pier seismic isolation for the Giant Magellan Telescope,” in [*Ground-based and Airborne Telescopes VII*], Marshall, H. K. and Spyromilio, J., eds., **10700**, 1759 – 1777, International Society for Optics and Photonics, SPIE (2018).
- [6] Baker, J. W., “Introduction to probabilistic seismic hazard analysis.” White Paper, Version 2.0.1 (2013) [https://web.stanford.edu/~bakerjw/Publications/Baker_\(2013\)_Intro_to_PSHA_v2.pdf](https://web.stanford.edu/~bakerjw/Publications/Baker_(2013)_Intro_to_PSHA_v2.pdf).
- [7] Constantinou, M., Mokha, A., and Reinhorn, A., “Teflon bearings in base isolation ii: Modeling,” *Journal of Structural Engineering* **116**(2), 455–474 (1990).
- [8] Schwartz, D., Feigum, K., Thompson, P. M., and Briggs, C., “Integrated modeling structural tools for the giant magellan telescope design effort,” in [*2018 IEEE Aerospace Conference*], 1–14 (2018).
- [9] Irarrazaval, B. A., Schwartz, D., Conan, R., Angeli, G., Bouchez, A. H., Das, K., and Quirós-Pacheco, F., “The Giant Magellan Telescope integrated modeling and performance (Conference Presentation),” in [*Modeling, Systems Engineering, and Project Management for Astronomy VIII*], Angeli, G. Z. and Dierickx, P., eds., **10705**, International Society for Optics and Photonics, SPIE (2018).